colorants

MDPI

Article

Preliminary in Silico Studies of the Interactions of Certain Genotoxic Azo Dyes with Different Double-Stranded DNA Conformations

Erman Salih İstifli

Department of Biology, Faculty of Science and Literature, Cukurova University, Adana TR-01330, Turkey; esistifli@cu.edu.tr; Tel.: +90-537-437-05-67

Abstract: Organic azo dyes, which are widely used in industrial, health and cosmetic fields, pose genotoxic risks due to their chemical structures; however, the molecular details of the undesirable effects of these dyes on DNA have been poorly or insufficiently clarified. In this computational molecular docking study, the DNA binding modes and binding affinities of 14 azo dyes, previously determined to show DNA clastogenicity, were characterized using 2 different double-stranded DNA (dsDNA) conformations (an *intact* dsDNA and dsDNA with an *intercalation gap*). In this study, it was determined that 10 out of the 14 genotoxic azo dyes were strong dsDNA minor groove binders, while the remaining ones formed tight binding complexes with dsDNA through intercalation or threading intercalation modes. The azo, nitro, hydroxyl, ammonium, sulfonate, naphthalene, methoxyphenyl, bromine, nitrophenyl, imidazole, amino-phenylethanol and chloro-nitrophenyl groups were found to play primary role in the most favorable binding conformations of these dyes on dsDNA with an affinity ranging from −6.35 kcal/mol to −9.42 kcal/mol. It was determined that dsDNA sequences containing GT dinucleotides are frequently preferred in binding by these dyes, and that rings and polar groups are important features for tight binding with dsDNA. It was concluded that these dyes may be banned, or non-genotoxic congeners should be manufactured with appropriate molecular optimization for the genetic health of the human population and for future generations.

Keywords: azo dyes; genotoxicity; dsDNA binding mode; molecular docking; human health

Citation: İstifli, E.S. Preliminary in Silico Studies of the Interactions of Certain Genotoxic Azo Dyes with Different Double-Stranded DNA Conformations. *Colorants* **2022**, *1*, 236–255. https://doi.org/10.3390/colorants1020015

Academic Editor: Anthony Harriman

Received: 20 March 2022
Accepted: 10 June 2022
Published: 14 June 2022

1. Introduction

Azo dyes are the largest colorant group, constituting 70% of all organic dyes produced in the world [1]. Simple synthesis protocols, large structural diversity, high molar extinction coefficients and medium-to-high fastness properties are the basis of such wide use of azo dyes [1]. The first azo dye, aniline yellow, was produced by Mene in 1861 [2]. On the other hand, dye production by diazotization and azo coupling method, as performed in modern industry today, was first performed in 1875 by Caro and Witt in Badische Aniline and Soda-Fabrik (BASF) [3].

Despite their widespread use around the world, serious biological effects of azo dyes, especially carcinogenic, mutagenic and genotoxic effects, have been consistently reported [4–8]. For instance, some industrial azo dyes are illegal additives that are frequently analyzed in foodstuffs. Although they do not have any nutritional value for the human body, they have toxic, carcinogenic and mutagenic effects that seriously harm consumer health [9].

While some azo dyes (4-aminoazobenzene, o-aminoazotoluene, methyl yellow and its derivatives, Sudan azo dyes and para red) are directly carcinogenic [10], others show carcinogenicity in the form of electrophilic metabolites (benzidine, p-phenylenediamine, etc.) [11]. Amido Black 10B, Basic red 51, Basic Brown 17, Disperse Red I, Disperse Red 13, Disperse Orange 1, Amaranth and Allura red were found to significantly increase the frequency of his^+ revertants in *Salmonella typhimurium*, induced primary DNA damage in

the comet test and micronucleus formation, and significantly upregulated genes involved in the inflammatory response, cell cycle control and apoptosis [12–16]. Acid Chrome Blue K, on the other hand, showed its genotoxic effect by binding to the grooves of the DNA in supercoiled plasmid pBR322 and by inducing the transition of the molecule to the nicked DNA form [17]. As can be seen, the structural alterations in the DNA molecule induced by azo dyes can adversely affect human health and jeopardize the molecular integrity of this molecule. If the abnormal structural changes that occur in DNA include genes that control the cell cycle, all these mutations, along with the disabling of apoptosis, can lead to the onset of malignant transformation [18–20]. Therefore, elucidation of the genotoxic action mechanisms of azo dyes at the molecular level is also of great importance in terms of public health.

DNA molecules are made up of two long polynucleotide chains consisting of four types of nucleotide subunits. Each of these chains is called a "*DNA strand*". The hydrogen bonds between the bases of the nucleotides hold the two chains together. Nucleotides consist of a five-carbon sugar attached to phosphate groups and a nitrogen-containing base. Bases in DNA can be adenine (A), thymine (T), cytosine (C) or guanine (G) [21–23].

As is known, small molecules interact with DNA through the mechanisms of intercalation or groove recognition [24,25]. Although the major groove of DNA contains more hydrogen bonding donor and acceptor sites, it is less favorable than the minor groove for binding of small molecules, and the majority of small ligands bind to minor grooves of DNA [25,26]. Among these binding modes, intercalation is the mode for small and rigid aromatic molecules to recognize DNA, while shape-selective agents generally bind to DNA through minor grooves similar to a *lock-and-key* mechanism [26,27]. In this context, although DNA is a known macromolecular target of azo dyes, studies characterizing the interaction of these dyes with DNA at the molecular level are not sufficient [28]. In silico structure–activity models have been acquiring more importance in elucidating the mechanisms of action of genotoxic small molecules. In this context, the molecular docking method offers unique advantages in harmonizing and correlating the data obtained from genotoxicity and cytotoxicity tests with structural information. Using this method, the visualization and analysis of the genotoxic mechanisms of small molecules at the molecular level can be performed reliably [29–31].

Therefore, in this study, double-stranded DNA (dsDNA) binding modes and affinities of certain genotoxic azo dyes, which were determined to interact or bind with dsDNA as a result of a detailed literature analysis, were studied by the molecular docking method. Two different dsDNA conformations were used to determine the dominant dsDNA binding modes of azo dyes: an *intact* dsDNA and dsDNA with a natural *intercalation gap*. The mechanistic information obtained as a result of this study provides a molecular-scale perspective on the dsDNA-damage-inducing potential of certain azo dyes.

2. Materials and Methods

2.1. Literature Filtering Criteria

Initially, we held the opinion that it would be useful to give information about the selection criteria of certain azo dyes which were simulated for dsDNA interactions in our study. In the literature filtering step, azo dyes showing experimental evidence of interacting with dsDNA were selected. For this purpose:

1. In the Web of Science database, a total of 84 research articles were found by using a combination of keywords "azo dye genotoxicity".
2. In the second step, among these 84 articles, further filtering was performed by using a combination of keywords, "genotoxicity DNA"; therefore, the total number of articles was reduced to 28. Thus, articles on the studies of azo dyes in which the genotoxic effect occurs due to intermolecular interactions with DNA were selected.

However, as is widely known, a positive result in genotoxicity/clastogenicity assay performed with cellular systems may not necessarily be an indication of the potential of the substance to cause direct DNA damage. Another point is that the induced lesions in DNA

in the comet assay can be efficiently repaired by the cell in a short time [32]. Therefore, a second criterion is whether the DNA damage revealed in genotoxicity tests is due to the direct interaction of the test substance with DNA [32–34]. Considering this point, the following further criteria were applied to rationalize the exact azo dye–DNA interaction:

a. In vivo micronucleus (MN) test result should be positive;
b. In vivo chromosome aberration (CA) test result should be positive;
c. Both in vitro comet and in vitro MN/CA test results should be positive;
d. Both in vivo comet and in vivo MN/CA test result should be positive;
e. Capability of forming DNA adducts in DNA-binding assays.

As a result, p-aminoazobenzene, o-aminoazotoluene, p-dimethylaminoazobenzene, phenazopyridine, Acid Chrome Blue K, Basic Red 51, Basic Brown 17, Amaranth, Allura Red, C.I. Disperse Blue 291, Amido Black 10B, C.I. Disperse Red 1, Disperse Orange 1 and Disperse Red 13 dyes were selected as certain DNA-reactive molecules to be simulated in molecular docking studies.

2.2. Receptor/Ligand Retrieval

In this study, azo compounds (Figure 1) (p-aminoazobenzene, o-aminoazotoluene, p-dimethylaminoazobenzene, phenazopyridine, Acid Chrome Blue K, Basic Red 51, Basic Brown 17, Amaranth, Allura Red, CI Disperse Blue 291, Amido Black 10B, CI Disperse Red 1, Disperse Orange 1 and Disperse Red 13), that were simulated based on their interactions with dsDNA, were downloaded in the sdf format from the PubChem database, National Library of Medicine (NIH). On the other hand, two receptor dsDNA molecules (PDB ID: 1MKL; resolution: not applicable; PDB ID: 1HJB; resolution: 3.00 Å) was downloaded from the RCSB Protein Data Bank in the pdb format. 1MKL is a 20-nucleotide dsDNA that possesses the intercalated aflatoxin B1 molecule (therefore, an *intercalation gap*) on its structure. On the other hand, the double-stranded crystallographic 1HJB consists of a total of 52 nucleotides in which the numerical distribution of A, T, G and C bases (14, 14, 12 and 12, respectively) are balanced; therefore, it does not possess a significant bias in favor of any nucleotide. Therefore, the 1HJB model isolated from *Homo sapiens* can be a preferable crystallographic structure in molecular docking simulations to better reflect the binding site preferences of azo compounds on the DNA molecule. The rationale for choosing two different dsDNA conformations—with and without an *intercalation gap*—in our study was to determine which binding mode (intercalative and groove binding) of azo dyes were more dominant.

2.3. Control Dockings

Control groups in molecular docking is important for success [35]. For this purpose, aflatoxin B1 (AFB1), a known DNA intercalator/minor groove binding agent, was used as the *positive control* in our study. In addition, as a *negative control*, aspirin (acetylsalicylic acid), a non-steroidal anti-inflammatory (NSAID) drug, which is experimentally proven to not interact strongly with DNA and to be non-genotoxic, was used [36–38]. Although the intercalative binding modes of both AFB1 and aspirin [39] have been reported in the literature, AFB1 can also interact with dsDNA through the minor groove binding mode [36,40]. Therefore, as described in the previous section, our docking simulations were performed using two different target conformations—dsDNA with an *intercalation gap* (1MKL) and an intact dsDNA (1HJB)—to avoid possible *false positive* or *false negative* binding poses. Thus, the different binding modes of AFB1 and aspirin arising from conformational changes in dsDNA have been revealed, and it has been shown which of these binding modes was energetically more favorable. Therefore, the *positive* and *negative control* groups used in our docking experiments ultimately provided a *validation* of the employed docking protocol.

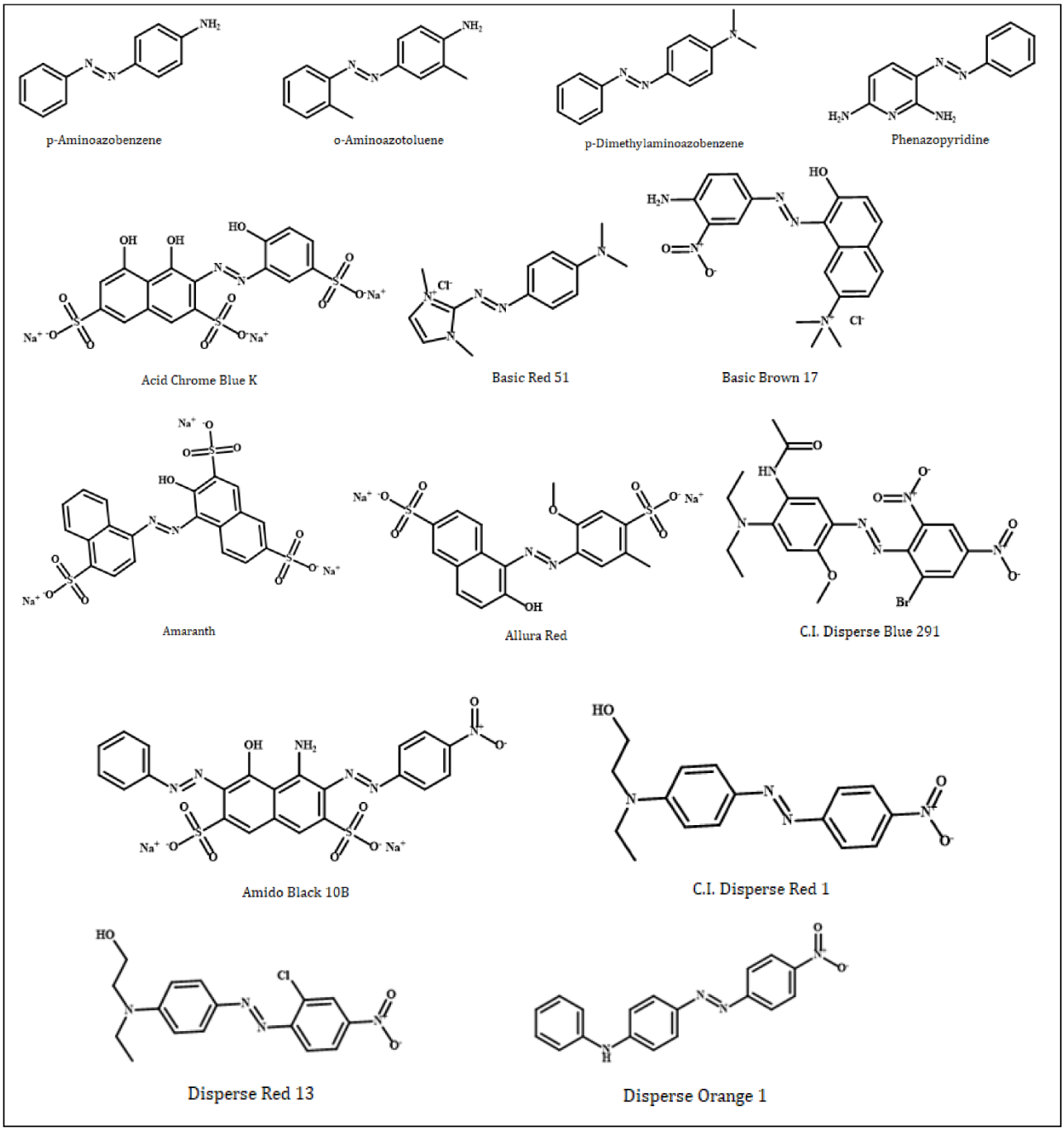

Figure 1. Two-dimensional chemical structures of genotoxic azo dyes. Structures were drawn using ChemOffice version 19.1.

2.4. Receptor/Ligand Preparation and Molecular Docking

In this study, 14 azo dyes (Table 1) and the *control* ligands downloaded from PubChem database in the sdf format were geometrically optimized using the Merck Molecular Force Field 94 (MMFF94) in the Avogadro program, and subsequently saved in pdb format [41]. MMFF94 is an efficient force field in the optimization of organic molecules [42] and provides reasonable accuracy in the geometric optimization of azo dyes and their metabolites [43,44]. On the other hand, the crystallographic dsDNA structures (1MKL and 1HJB) used as the target receptors in our study were prepared by removing the bound ligand and protein complexes in the Discovery Visual Studio v16 program and recorded in pdb format prior to docking.

Table 1. PubChem CID, molecular weight and molecular formula of the genotoxic azo dyes and their metabolites.

No	Compound	PubChem CID	Molecular Weight (g/mol)	Molecular Formula
		Genotoxic azo dyes		
1	p-Aminoazobenzene	6051	197.24	$C_{12}H_{11}N_3$
2	o-Aminoazotoluene	7340	225.29	$C_{14}H_{15}N_3$
3	p-Dimethylaminoazobenzene	6053	225.29	$C_{14}H_{15}N_3$ or $C_6H_5N{=}NC_6H_4N(CH_3)_2$
4	Phenazopyridine	4756	213.24	$C_{11}H_{11}N_5$
5	Acid Chrome Blue K	135659037	586.4	$C_{16}H_9N_2Na_3O_{12}S_3$
6	Basic Red 51	166491	279.77	$C_{13}H_{18}ClN_5$
7	Basic Brown 17	135515517	401.8	$C_{19}H_{20}ClN_5O_3$
8	Amaranth	13506	604.5	$C_{20}H_{11}N_2O_{10}S_3.3Na$ or $C_{20}H_{11}N_2Na_3O_{10}S_3$
9	Allura Red	33258	496.4	$C_{18}H_{14}N_2Na_2O_8S_2$
10	C.I. Disperse Blue 291	92446	509.3	$C_{19}H_{21}BrN_6O_6$
11	Amido Black 10B	135442942	616.5	$C_{22}H_{14}N_6Na_2O_9S_2$
12	C.I. Disperse Red 1	17886	314.34	$C_{16}H_{18}N_4O_3$
13	Disperse Orange 1	17414	318.3	$C_{18}H_{14}N_4O_2$
14	Disperse Red 13	18516	348.78	$C_{16}H_{17}ClN_4O_3$

For molecular modelling, the new AutoDock Vina (version 1.2.0, Center of Computational Structural Biology—Scripps Research, La Jolla, CA, USA) was used to perform rigid receptor–flexible ligand docking simulations in our study. Along with AutoDock4 (AD4), AutoDockGPU, AutoDockFR and AutoDock-CrankPep, AutoDock Vina (Vina) is one of the docking engines in the AutoDock Suite and is among the most widely used and successful docking programs in the world. The reasons for this success are its ease of use, speed (up to 100 times faster than AD4) and open source code, both in the suite and when compared with other docking programs [45].

In the molecular docking studies of azo dyes against two different dsDNA conformations, polar hydrogen atoms in receptor and ligand molecules were retained, while nonpolar hydrogens were merged and then the Gasteiger charges of the ligands were calculated with AutoDockTools, as previously described [46]. On the other hand, the Kollmann charges were added for the target receptors. During the docking experiments, all the rotatable bonds of the azo dyes and control ligands were allowed to rotate freely, and the prepared dsDNA and ligand structures were saved in PDBQT format. Two different grid box sizes were determined in dockings with two different dsDNA conformers: 90 × 90 × 90 Å points (x: 118.9; y: 93.2; z: 14.1) for dsDNA with an *intercalation gap*; 80 × 80 × 160 Å points (x: 24.8; y: 91.3; z: 4.6) for *intact* dsDNA, using a grid spacing of 0.375 Å. These grid box sizes included the entire dsDNA structure as the search space and adequately covered all the major and minor grooves of these target receptors.

For all ligands and controls, 2 separate docking runs were performed (40 dockings for each ligand with an *exhaustiveness* value of 200) against 2 different dsDNA conformations. Following docking, all potential binding modes of the ligands were clustered by AutoDock Vina 1.2.0 and were ranked based on the binding affinity (ΔG°; kcal/mol) of the ligand conformation which showed the lowest binding free energy against the dsDNA targets. The Best-ranked conformation of the ligands obtained by AutoDock Vina 1.2.0 among different poses on the targets was visualized and analyzed using Discovery Studio Visualizer v16.

3. Results and Discussion

3.1. Control Dockings

In this study, aflatoxin B1 (AFB1) and aspirin (acetylsalicylic acid) were used as internal controls for the validation of the docking protocol. Control calculations are important to the

success of docking experiments; control molecules are useful in distinguishing real active molecules from real inactive molecules [35]. The *positive control* molecule AFB1 exhibited intercalation and minor groove binding mode in dsDNA (Table 2), and both modes of binding are consistent with the literature [36,40]. However, the dsDNA intercalation mode of AFB1 was energetically more favorable ($\Delta G^\circ = -8.64$ kcal/mol) (Figure 2a, Table 2). The *negative control* aspirin binds energetically favorably to both dsDNA conformations (*intact* dsDNA, dsDNA with *intercalation gap*), whereas it binds more favorably ($\Delta G^\circ = -6.10$ kcal/mol) to dsDNA with an *intercalation gap* (Figure 2b, Table 2). The docking conformation of aspirin is in agreement with the reported experimental data. A previous spectroscopic and docking study showed that the dominant binding mode of aspirin to DNA was intercalative [39]. Therefore, *positive* and *negative control* ligands (AFB1 and aspirin) that we used in our study provided validation for further docking simulations with azo compounds.

Table 2. Docking results of 14 genotoxic azo dyes and control compounds showing the binding free energy (BFE), dual binding mode and intermolecular interactions with dsDNA.

Dye (Ligand)	BFE (kcal/mol)	Binding Mode	Intermolecular Interactions
AFB1 (*positive control*)	−8.64	Intercalation	1 carbon–hydrogen bond (Cyt15), 9 pi–pi stacked (Cyt5, Gua6, Gua16)
	−8.12	Minor groove	3 H bonds (Ade11, Gua18)
Aspirin (*negative control*)	−6.10	Intercalation	1 H bond (Gua6), 6 pi–pi stacked (Cyt5, Gua6, Cyt15, Gua16)
	−5.77	Minor groove	4 H bonds (Gua18, Thy19, Gua20)
p-Aminoazobenzene	−6.49	Intercalation	2 H bonds (Gua6), 6 pi–pi stacked (Cyt5, Gua6, Gua16, Cyt15)
	−6.45	Minor groove	3 H bonds (Gua12, Cyt16, Thy17), 1 pi–donor H bond (Gua12)
o-Aminoazotoluene	−6.92	Threading intercalation	1 H bond (Gua16), 6 pi–pi stacked (Cyt5, Gua6, Cyt15, Gua16), 2 pi–pi T-shaped (Gua6, Ade7), 5 pi–alkyl (Cyt5, Gua6, Cyt15, Gua16)
	−6.73	Minor groove	2 H bonds (Gua12, Thy17)
p-Dimethylaminoazobenzene	−6.50	Threading intercalation	1 carbon–hydrogen bond (Gua16), 6 pi–pi stacked (Cyt5, Gua6, Cyt15, Gua16), 1 pi–pi T-shaped (Gua6)
	−6.66	Minor groove	3 H bonds (Ade11, Gua18, Thy19), 1 carbon–hydrogen bond (Ade11)
Phenazopyridine	−6.69	Intercalation	2 H bonds (Cyt15, Gua16), 1 pi–donor H bond (Gua16), 6 pi–pi stacked (Cyt5, Gua6, Cyt15, Gua16)
	−6.94	Minor groove	4 H bonds (Gua18, Thy19, Gua20), 1 carbon–hydrogen bond (Ade11)
Acid Chrome Blue K	−8.71	Threading intercalation	4 H bonds (Cyt5, Gua6, Ade7, Cyt15), 1 carbon–hydrogen bond (Cyt15), 11 pi–pi stacked (Cyt5, Gua6, Cyt15, Gua16)
	−9.36	Minor groove	6 H bonds (Ade9, Cyt10, Ade13, Gua18, Gua20), 3 carbon–hydrogen bonds (Gua12, Thy19, Gua20), 1 pi–sulfur (Ade9)

Table 2. *Cont.*

Dye (Ligand)	BFE (kcal/mol)	Binding Mode	Intermolecular Interactions
Basic Red 51	−6.94	Threading intercalation	2 carbon–hydrogen bonds (Ade7, Gua16), 1 pi–donor hydrogen bond (Gua6), 6 pi–pi stacked (Cyt5, Gua6, Cyt15, Gua16)
	−6.35	Minor groove	1 H bond (Gua12), 1 carbon–hydrogen bond (Cyt16)
Basic Brown 17	−8.50	Threading intercalation	2 H bonds (Ade7, Cyt15), 2 carbon–hydrogen bonds (Gua6), 1 pi–donor hydrogen bond (Gua6), 9 pi–pi stacked (Cyt5, Gua6, Cyt15, Gua16)
	−8.79	Minor groove	1 attractive charge (Thy19), 6 H bonds (Ade11, Ade13, Cyt16, Thy17, Gua18), 2 carbon–hydrogen bonds (Gua18)
Amaranth	−8.74	Threading intercalation	4 H bonds (Gua6, Cyt15, Gua16), 1 pi–sulfur (Ade7), 11 pi–pi stacked (Cyt5, Gua6, Cyt15, Gua16), 1 pi–pi T-shaped (Ade7)
	−9.42	Minor groove	5 H bonds (Ade9, Gua12, Thy17, Gua20, Gua21), 1 carbon–hydrogen bond (Gua12), 1 pi–donor hydrogen bond (Ade11), 1 pi–sulfur (Gua20)
Allura Red	−8.19	Intercalation	1 H bond (Cyt15), 1 carbon–hydrogen bond (Gua16), 1 pi–donor hydrogen bond (Gua6), 10 pi–pi stacked (Cyt5, Gua6, Cyt15, Gua16), 2 pi–alkyl (Cyt5, Gua6)
	−8.80	Minor groove	5 H bonds (Ade9, Ade11, Gua12, Gua20, Gua21), 1 carbon–hydrogen bond (Gua12), 1 pi–sulfur (Gua20)
C.I. Disperse Blue 291	−7.39	Threading intercalation	2 H bonds (Gua6, Cyt15), 3 carbon–hydrogen bond (Cyt15, Ade17), 6 pi–pi stacked (Cyt5, Gua6, Cyt15, Gua16), 3 pi–alkyl (Cyt15, Gua16)
	−6.90	Major groove	4 H bonds (Ade13, Cyt14), 1 pi–pi T-shaped (Gua14), 1 Pi–alkyl (Gua14)
Amido Black 10B	−8.30	Threading intercalation	4 H bonds (Cyt15, Gua16), 6 pi–pi stacked (Cyt5, Gua6, Cyt15, Gua16)
	−9.23	Minor groove	7 H bonds (Ade5, Thy22, Thy23, Gua24), 2 pi–pi T-shaped (Gua21, Gua24)
C.I. Disperse Red 1	−6.94	Threading intercalation	6 pi–pi stacked (Cyt5, Gua6, Cyt15, Gua16)
	−7.67	Minor groove	3 H bonds (Ade9, Gua20), 1 pi–donor hydrogen bond (Ade11)
Disperse Orange 1	−8.18	Threading intercalation	6 pi–pi stacked (Cyt5, Gua6, Cyt15, Gua16)
	−8.23	Minor groove	3 H bonds (Ade9, Gua20)
Disperse Red 13	−7.27	Threading intercalation	1 pi–donor hydrogen bond (Gua6), 1 pi–sigma (Gua16), 6 pi–pi stacked (Cyt5, Gua6, Cyt15, Gua16), 2 pi–alkyl (Cyt15, Gua16)
	−7.68	Minor groove	4 H bonds (Ade9, Gua12, Gua20)

BFE: Binding free energy (kcal/mol).

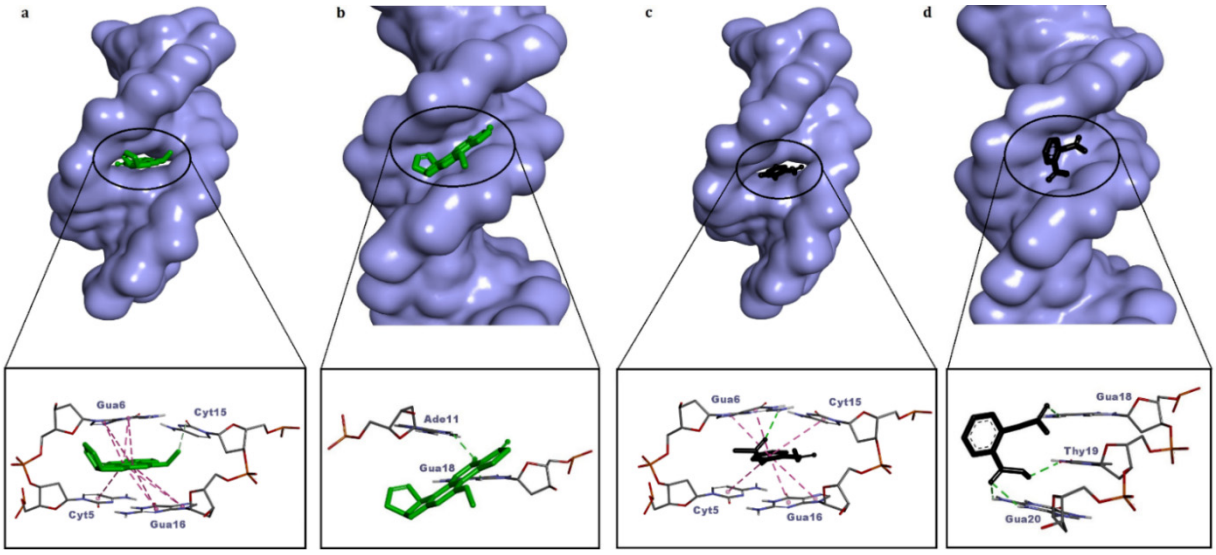

Figure 2. Molecular surface view of the best-ranked conformations of aflatoxin B1 (**a**,**b**) and aspirin (**c**,**d**) on two different conformations of dsDNA (with and without an *intercalation gap*) and 3D ligand–dsDNA interaction diagrams. Notice that both the controls, aflatoxin B1 and aspirin, are snugly fitted on the dsDNA with an intercalation gap (**a**,**c**).

3.2. Molecular Docking against Intact dsDNA and dsDNA with Natural Intercalation Gap

In our study, the docking calculations of 14 azo dyes (p-aminoazobenzene, o-aminoazotoluene, p dimethylaminoazobenzene, phenazopyridine, Acid Chrome Blue K, Basic Red 51, Basic Brown 17, Amaranth, Allura Red, C.I. Disperse Blue 291, Amido Black 10B, C.I. Disperse Red 1, Disperse Orange 1, Disperse Red 13), which were confirmed to be genotoxic as a result of a comprehensive literature review, were performed against two different dsDNA conformations: an *intact* dsDNA and dsDNA with an *intercalation gap*. Since the docking simulations using a single receptor conformation can be misleading in terms of the real binding mode of the molecule, such an approach could be used as a strategy to determine which binding mode is energetically more favorable.

P-aminoazobenzene interacted with both dsDNA conformations (*intact* dsDNA and dsDNA with an *intercalation gap*) with very close binding affinities ($\Delta G^\circ = -6.45$ kcal/mol; $\Delta G^\circ = -6.49$ kcal/mol, respectively) (Table 2). While hydrogen bonds were more numerous in the interaction of p-aminoazobenzene with the minor groove of *intact* dsDNA, hydrophobic pi–pi stacking interactions played the most important role in binding with dsDNA carrying an *intercalation gap* (Table 2). While the interaction with the minor groove was through the phenyl, azo and aniline groups of p-aminoazobenzene, azo and aniline groups, on the other hand, played an important role in the snug fit of this ligand into the dsDNA with an *intercalation gap* (Figures 3a,b and 4a,b). O-aminoazotoluene was slightly favorably bound to dsDNA containing an *intercalation gap* compared with the *intact* dsDNA ($\Delta G^\circ = -6.92$ kcal/mol; $\Delta G^\circ = -6.73$ kcal/mol, respectively) (Table 2). Hydrophobic stacked pi–pi and pi–alkyl interactions played the most important role in the interaction of o-aminoazotoluene with dsDNA carrying an *intercalation gap*. On the other hand, hydrogen bonds played a dominant role in the interaction with the minor groove of intact dsDNA (Table 2). While 2-methyl aniline and 2-methyl phenyl groups were effective in the *threading intercalation* of o-aminoazotoluene, only the azo (–N=N–) structure was effective in the interaction of this ligand with the minor groove of intact dsDNA (Figures 3c,d and 4c,d). In the interaction of p-dimethylaminoazobenzene with the dsDNA molecule, the dsDNA affinity of the intercalation (threading) and minor groove binding modes were quite close to each other ($\Delta G^\circ = -6.50$ kcal/mol; $\Delta G^\circ = -6.66$ kcal/mol, respectively) (Table 2). While hydrophobic pi–pi interactions played the most important role in the snug fit of this ligand to the dsDNA containing the *intercalation gap*, the

minor groove recognition mode basically occurred through the formation of H bonds (Table 2). Moreover, it was found that the aniline group was effective in the threading type intercalation of p-dimethylaminoazobenzene on dsDNA, while the azo (–N=N–) structure was effective in convergence and binding to DNA via the minor groove recognition (Figures 3e,f and 4e,f). In the intermolecular interaction of phenazopyridine with the dsDNA molecule, the minor groove binding mode was slightly more favorable than the intercalative binding ($\Delta G^\circ = -6.94$ kcal/mol; $\Delta G^\circ = -6.69$ kcal/mol, respectively) (Table 2). While hydrogen bonds played the dominant role in the interaction of phenazopyridine with the minor groove of the dsDNA molecule, H bonds and hydrophobic pi–pi interactions are prominent in the intercalative binding mode of this ligand (Table 2). The minor groove binding mode of this ligand was mediated by azo and amine groups, while azo, pyridine and amine groups played a dominant role in the intercalative binding of phenazopyridine (Figures 3g,h and 4g,h).

In an in vivo comet assay conducted with eight different mouse organs, p-aminoazobenzene, o-aminoazotoluene, p-dimethylaminoazobenzene and phenazopyridine caused DNA fragmentation in the stomach, colon, lung, urinary bladder, brain and bone marrow, and also caused tumor formation in the liver, lung, urinary bladder and colon [47]. While there is no correlation between the genotoxic potency and the number of azo bonds for these four compounds, the exocyclic amino group of these derivatives (even other azo dyes which possess this group) has been shown to be the critical unit for genotoxicity or carcinogenicity, as it undergoes *N*-oxidation by cytochrome P450 in the liver to form reactive electrophiles that induce the formation of DNA adducts [48–50]. This reported literature data is also in agreement with our docking results, as exocyclic amino groups showed efficacy in the most energetically favorable interactions of these four ligands against the dsDNA (Table 2, Figure 3a–h).

In the intermolecular interaction of Acid Chrome Blue K (ACBK) with the dsDNA, the minor groove binding mode was considerably more favorable compared with the intercalative binding ($\Delta G^\circ = -9.36$ kcal/mol; $\Delta G^\circ = -8.71$ kcal/mol, respectively) (Table 2). H bonds played an important role in the minor groove recognition of ACBK with the dsDNA molecule, while H bonds and hydrophobic pi–pi stacking contacts were more prominent in the intercalative (threading) binding mode of this ligand (Table 2). The minor groove binding mode of this ligand was mediated by sulfonic, naphthalene (hydroxyl groups) and phenol groups (hydroxyl groups); meanwhile, sulfonic and naphthalene rings played a dominant role in its intercalative binding mode (Figures 3i,j and 4i,j). Although there are no adequate studies on the genotoxicity of ACBK in the literature, in a DNA binding assay conducted using plasmid pBR322 DNA, it was found that ACBK was snugly fit into the minor groove of DNA, and the hydroxyl and sulfonic acid moieties have been reported to play a primary role in this binding mode [17]. Additionally, it was shown that an efficient DNA strand cleavage occurred in the presence of a high concentration of ACBK in the irradiated plasmid DNA [17]. These experimental results are in excellent agreement with our docking study, since the dsDNA minor groove binding mode of ACBK had occurred primarily through sulfonic acid and hydroxyl groups; furthermore, the minor groove binding mode of ACBK was energetically quite favorable based on the docking experiment (Table 2, Figure 3i,j).

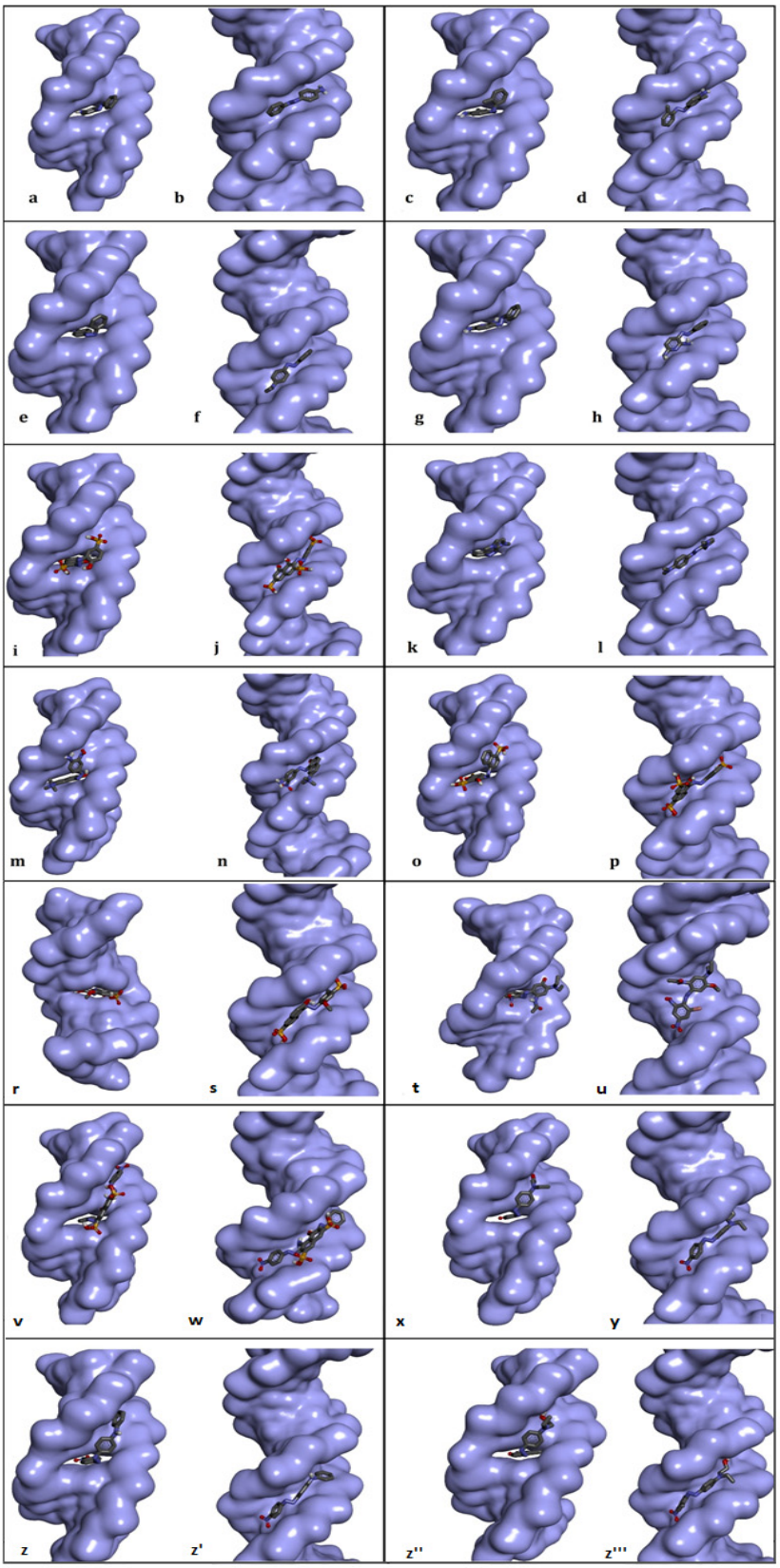

Figure 3. Best-ranked conformations of the genotoxic azo dyes with dsDNA in two distinct conformations (with and without an *intercalation gap*) (**a**–**z'''**). dsDNA molecule is represented as surface and ligands are depicted in stick mode. P-aminoazobenzene (**a**,**b**), o-aminoazotoluene (**c**,**d**), p-dimethylaminoazobenzene (**e**,**f**), phenazopyridine (**g**,**h**), Acid Chrome Blue K (**i**,**j**), Basic Red 51 (**k**,**l**), Basic Brown 17 (**m**,**n**), Amaranth (**o**,**p**), Allura red (**r**,**s**), C.I. Disperse Blue 291 (**t**,**u**), Amido Black 10B (**v**,**w**), C.I. Disperse Red 1 (**x**,**y**), Disperse Orange 1 (**z**,**z'**), Disperse Red 13 (**z''**,**z'''**).

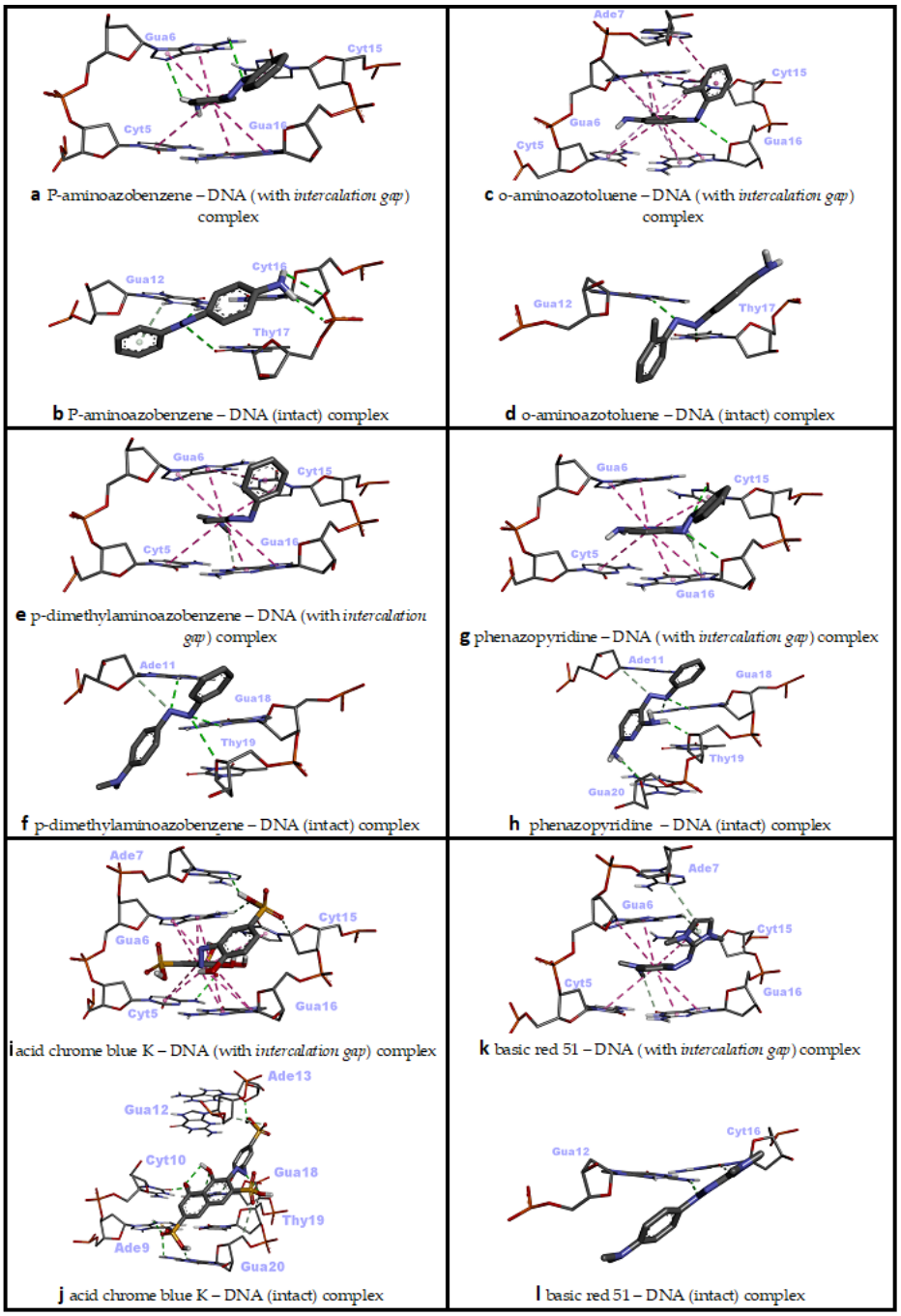

Figure 4. Two-dimensional interaction diagrams of genotoxic azo dyes with dsDNA in two distinct conformations (with and without an *intercalation gap*). dsDNA structures and ligands are depicted in stick mode.

In the intermolecular interaction of Basic Red 51 with the dsDNA molecule, the intercalative (threading) binding mode was more favorable than minor groove recognition ($\Delta G^\circ = -6.94$ kcal/mol; $\Delta G^\circ = -6.35$ kcal/mol, respectively) (Table 2). While H bonds and hydrophobic pi–pi-stacked contacts played an important role in the intercalative binding mode of Basic Red 51 against the dsDNA molecule, H bonds were more prominent in the minor groove binding mode of this ligand (Table 2). The mode of intercalative binding of this ligand to dsDNA was mediated by the imidazole ring, phenyl, and tertiary amine (on the phenyl), while azo and imidazole rings played a dominant role in the minor groove binding (Figures 3k,l and 4k,l). In the in vitro comet and cytokinesis-blocked micronucleus tests performed on HepG2 cells, Basic Red 51 significantly increased DNA

damage (DNA fragmentation and micronucleus, respectively) compared with the control group. Researchers have suggested that the resulting clastogenic damage may be partially due to the azo group in the dye [16]. In our docking study, imidazole ring, phenyl and tertiary amine were the groups shown to be effective in intercalation (Figure 3k,l), which is, energetically, the most favorable binding conformation of Basic Red 51 against the dsDNA.

However, considering that the cellular DNA used in the reported study does not contain intercalation gaps, minor groove binding and thus the effect of azo and imidazole groups may also be responsible for the induced genotoxicity in HepG2 cells [16].

In the interaction of Basic Brown 17 with dsDNA, the minor groove recognition was more efficient than the intercalative (threading) binding mode, and in the minor groove recognition mode, Basic Brown 17 showed a very high binding affinity with dsDNA ($\Delta G^\circ = -8.79$ kcal/mol; $\Delta G^\circ = -8.50$ kcal/mol, respectively) (Table 2). While H bonds and electrostatic interactions played the dominant role in the groove recognition mode, hydrophobic pi–pi-stacked contacts and H bonds were active in Basic Brown 17's intercalative binding mode (Table 2).

The nitro, azo, hydroxyl and ammonium groups were effective in the minor groove recognition of this ligand, whereas the ammonium, naphthalene and its hydroxyl group, and 2-nitroaniline moieties in the molecular structure of Basic Brown 17 played significant role in the intercalative binding mode with dsDNA (Figures 3m,n and 5a,b). Basic Brown 17 significantly induced the formation of DNA fragments at all concentrations used in the in vitro comet test and chromosomal damage in the micronucleus test in HepG2 cells [16]. Researchers attributed DNA damage induced by Basic Brown 17 partially to the azo group (R–N=N–R′) in its structure. These reported results are in agreement with our docking study, as the azo group, as well as the nitro, hydroxyl and ammonium groups, are active in minor groove recognition, which is the most favorable binding mode of this agent with dsDNA (Table 2). The results obtained from the docking of Basic Brown 17 also show that the docking conformational search can produce the correct molecule orientation compatible with the experimental results.

Amaranth's interaction with dsDNA through the minor groove was considerably stronger compared with the intercalative (threading) mode and exhibited a very high binding affinity for dsDNA in the minor groove recognition mode ($\Delta G^\circ = -9.42$ kcal/mol; $\Delta G^\circ = -8.74$ kcal/mol, respectively) (Table 2). Basically, many H bonds were effective in Amaranth's snug fit to the minor groove, while a large number of hydrophobic pi–pi contacts and a small amount of H bonds played a role in the intercalation mode (Table 2). While sulfonate, hydroxyl groups and naphthalene rings in its molecular structure played a significant role in the minor groove binding mode of Amaranth, sulfonate and naphthalene rings were effective in the intercalative binding mode (Figures 3o,p and 5c,d). Amaranth can bind to DNA as shown by UV–vis experiments in which a distinct isosbestic point at 297 nm was observed, suggesting binding of the dye to the DNA [51]. Additionally, Amaranth induced chromosomal damage (specially chromatid breaks) in Chinese hamster fibroblast cell line and increased single-strand DNA breakage in *Saccharomyces cerevisiae* in the comet assay [15,51]. These results are in agreement with our docking study, because Amaranth formed highly stable complexes with both *intact* dsDNA and the dsDNA carrying an *intercalation gap*. However, the type of dsDNA damage that may occur (single- or double-strand DNA breaks) depends highly on the cell cycle phase in which Amaranth interacts with cellular DNA.

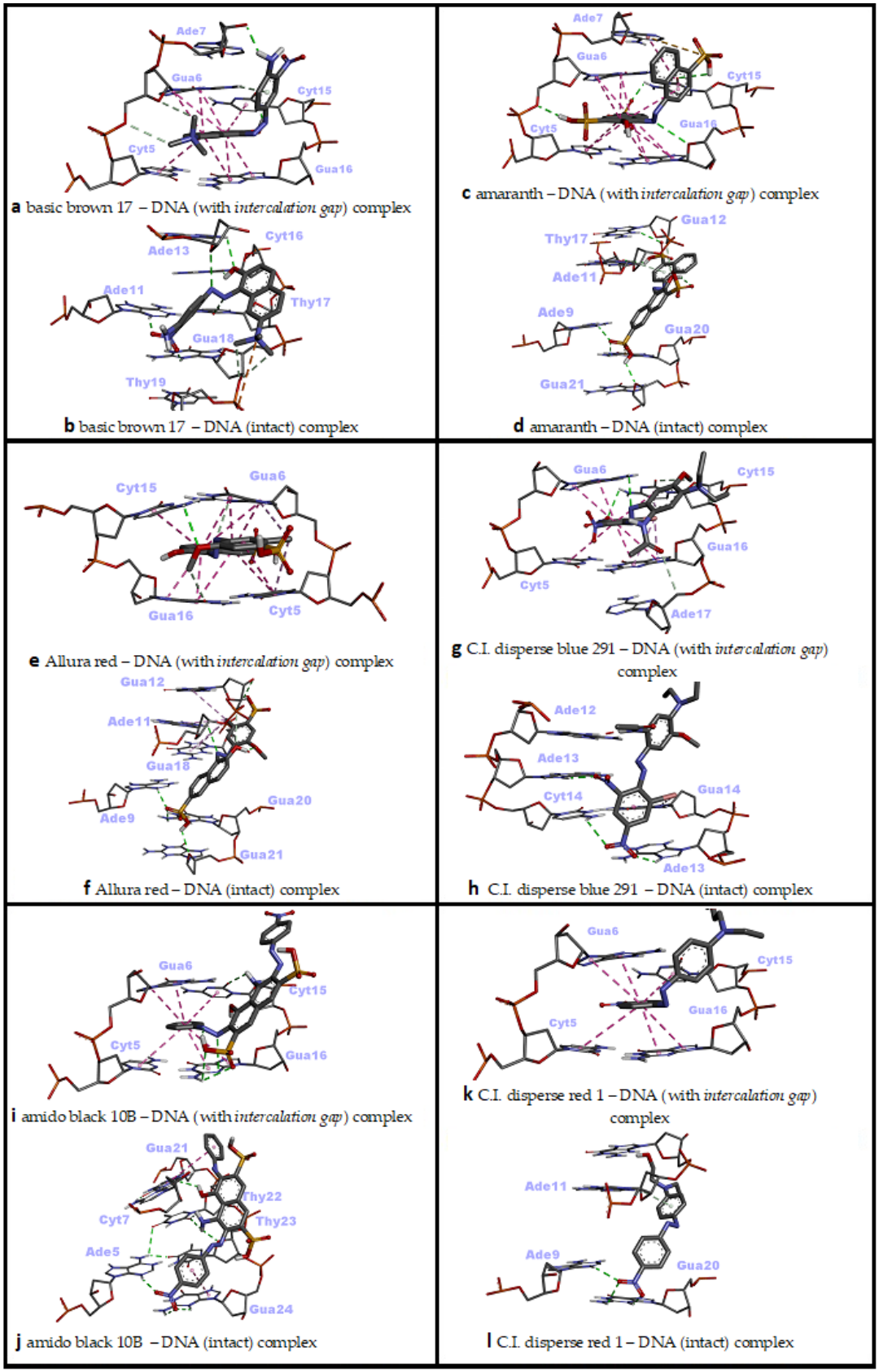

Figure 5. Two-dimensional interaction diagrams of genotoxic azo dyes with dsDNA in two distinct conformations (with and without an *intercalation gap*). dsDNA structures and ligands are depicted in stick mode.

In the docking simulation of Allura Red, minor groove recognition was more favorable than the intercalative binding mode, and it exhibited a very favorable binding affinity for dsDNA ($\Delta G^\circ = -8.80$ kcal/mol; $\Delta G^\circ = -8.19$ kcal/mol, respectively) (Table 2). While H bonds were mainly active in the conformational fit of Allura Red to the minor groove, a large number of hydrophobic pi–pi contacts and a small amount of H bonds played role in the intercalation mode (Table 2). The sulfonate, azo and naphthalene ring-bound hydroxyl groups in the molecular structure played the main role in Allura Red's minor groove recognition, while the planar rings of naphthalene and methoxy phenyl were effective in the intercalative binding mode (Figures 3r,s and 5e,f). It has been reported that Allura Red significantly increased DNA fragmentation (single-strand DNA breaks) between 1250 and 5000 microgram/mL concentrations (at 37 °C) compared with the control in the comet assay of *Saccharomyces cerevisiae* [15]. The dsDNA binding affinity of Allura Red in the docking simulation correlate with the reported formation of experimental DNA breaks. Allura red forms very stable complexes with dsDNA in both the minor groove and intercalative binding modes, and these complexes are able to induce DNA strand breaks which could be due to changes in DNA conformation or DNA torsional tension.

In the docking simulation of C.I. Disperse Blue 291 (CIDB291), intercalation (threading), which is the primary dsDNA binding mode, was more potent than the major groove binding mode ($\Delta G^\circ = -7.39$ kcal/mol; $\Delta G^\circ = -6.90$ kcal/mol, respectively) (Table 2). In the intercalative binding mode of CIDB291, H bonds were mainly active along with hydrophobic pi–pi and pi–alkyl contacts, while H bonds and a small number of hydrophobic pi–pi and pi–alkyl interactions played a role in the major groove binding mode (Table 2). In the intercalative (threading) binding mode of CIDB291, the phenyl ring and the bromine atom attached to it, as well as the amide and methoxy groups attached to the second phenyl ring played significant role, while the phenyl ring, nitro groups, bromine atom and amide group were effective in the major groove binding mode of this dye (Figures 3t,u and 5g,h). According to our docking results, although CIDB291 has the capacity to bind tightly to dsDNA in its native conformation (most probably via *intercalation*), acetylated hydroxylamines, which are formed as a result of the metabolic process of CIDB291 by nitro reductase and o-acetyl transferases, have been reported to interact with DNA and pose a mutagenic effect [52]. In addition, it has been reported that genotoxic intermediates of this dye may also occur as a result of the metabolism of -OCH_3 and -$N(CH_2CH_3)_2$) substituents by cytochrome P450 [52]. Therefore, in addition to its native conformation, electrophilic nucleophiles (metabolites) that occur as a result of its metabolism in the host organism play the primary role in the genotoxic effect of CIDB291.

In the docking simulation of Amido Black 10B (AB10B), minor groove recognition, the primary dsDNA binding mode, was highly more potent than the intercalative (threading) mode ($\Delta G^\circ = -9.23$ kcal/mol; $\Delta G^\circ = -8.30$ kcal/mol, respectively) (Table 2). In the minor groove binding mode of AB10B, many H bonds as well as hydrophobic pi–pi T-shaped contacts were active, while hydrophobic pi–pi stacking interactions and small number of H bonds played role in the intercalative binding mode of AB10B (Table 2). In the minor groove binding mode of AB10B, the nitrophenyl ring, the naphtalene moiety with bound amino and hydroxyl groups, as well as the second phenyl ring of the molecule played significant role, while the phenyl ring, azo, nitro and amine groups were effective in the intercalative binding mode of this agent (Figures 3v,w and 5i,j). In a recent experimental study, it was reported that AB10B increased his^+ revertants in *Salmonella* TA98 strain in a dose-dependent manner, while significantly increasing single-/double-strand DNA breaks and micronucleus and nuclear bud formation in human liver HepG2 cell line [12]. These results are in good agreement with our docking study. AB10B can induce single- and double-strand breaks due to its strong affinity to dsDNA ($\Delta G^\circ = -9.23$ kcal/mol in the minor groove binding mode), and these breaks give positive results in the comet and micronucleus test. The simultaneous induction of single and double strand breaks by AB10B indicates that this azo dye can induce DNA strand breaks in both G_1 and S phases of the cell cycle.

However, according to our docking results, it is also possible for AB10B to induce DNA damage by binding to dsDNA in the intercalation mode ($\Delta G^\circ = -8.30$ kcal/mol).

In the docking simulation of C.I. Disperse Red 1 (CIDR1) against dsDNA, it was determined that minor groove recognition was the primary DNA binding mode and was energetically more favorable than the intercalative (threading) binding mode ($\Delta G^\circ = -7.67$ kcal/mol; $\Delta G^\circ = -6.94$ kcal/mol, respectively) (Table 2). In the minor groove binding mode of CIDR1, H bonds were predominant, while hydrophobic pi–pi stacking interactions and one H bond were effective in the intercalative (threading) binding mode of CIDR1 (Table 2). In the minor groove binding mode of CIDR1, the nitrophenyl moiety and phenyl aminoethanol moiety carrying a hydroxyl group played significant role, while only the phenyl group of the nitrophenyl moiety was effective in the intercalative binding mode of this agent with dsDNA (Figures 3x,y and 5k,l). The DNA-damaging mechanism of CIDR1 is still unknown; however, it is thought that the native molecule of this commercial dye as well as the electrolytic oxidation and reduction products affect the double-helix structure of DNA, causing conformational changes and subsequent genomic damage [53,54]. This hypothesis is also consistent with our docking results, as CIDR1 can form a very tight binding complex ($\Delta G^\circ = -7.67$ kcal/mol) with dsDNA in the minor groove recognition mode, which could lead to DNA breaks in either the G_1 or S phase (single- and double-strand breaks, respectively) of the cell cycle. Consistent with this hypothesis, it was found that CIDR1 significantly increased the rate of micronucleated polychromatic erythrocytes (MNPCE) in Swiss mice bone marrow cells and primary DNA damage in the comet assay compared with the control [13].

In the molecular docking simulation of Disperse Orange 1 (DO1), performed with two different dsDNA conformations, minor groove recognition and intercalation (threading) binding modes were found to be energetically close to each other and both were favorable ($\Delta G^\circ = -8.23$ kcal/mol; $\Delta G^\circ = -8.18$ kcal/mol, respectively) (Table 2).

In the minor groove binding mode of DO1, H bonds were predominant, while numerous hydrophobic pi–pi stacking interactions and few H bonds were effective in the intercalative (threading) binding mode of DO1 (Table 2). In the minor groove binding mode of DO1, the nitro group bound to nitrophenyl moiety played significant role, while the planar phenyl ring of the same moiety was effective in the intercalative binding mode of DO1 to dsDNA (Figures 3z,z' and 6a,b). Consistent with our docking study, in a UV–vis spectrophotometric study, it was reported that DO1 and its electrolysis product predominantly bound to the immobilized dsDNA via intercalation mode and damaged the biomolecule [53]. Researchers have reported that local structural changes, such as unwinding of the double helix and lengthening of the DNA strand, are the basis of this damage, which, in turn, lead to retardation or inhibition of transcription and replication [53].

When the docking affinities of the last ligand, Disperse Red 13 (DR13) were compared against two different dsDNA conformations, it was determined that the minor groove recognition mode was energetically slightly more favorable than the intercalative (threading) binding mode ($\Delta G^\circ = -7.68$ kcal/mol; $\Delta G^\circ = -7.27$ kcal/mol, respectively) (Table 2). In the minor groove binding mode of DR13, H bonds were effective, while numerous hydrophobic pi–pi stacking, pi–alkyl and pi–sigma interactions as well as one H bond were effective in the intercalative (threading) binding mode of DR13 (Table 2). The nitro group bound to chloro-nitrophenyl moiety and the hydroxyl of phenyl-aminoethanol moiety played significant role in the minor groove binding mode of DR13, while the two phenyl rings of chloro-nitrophenyl and phenyl-aminoethanol moieties were effective in the intercalative binding mode of DR13 to dsDNA (Figures 3z'',z''' and 6c,d). Although there is no mechanistic study of the DNA binding mechanism of DR13, it has been reported that chlorinated DR13 increases DNA damage in the comet test performed with human liver HepG2 cells in a dose-dependent manner [14]. Although the result obtained from this study is also in agreement with our docking study on the basis of DNA reactivity, additional binding studies are needed regarding the actual DNA interaction mode of DR13. In this study, the entire calculated binding affinities of 14 azo dyes by AutoDock Vina 1.2.0 and the

structural differences (RMSD—root mean square deviation) between these binding poses against each DNA conformation can be found in the Supplementary Materials Table S1.

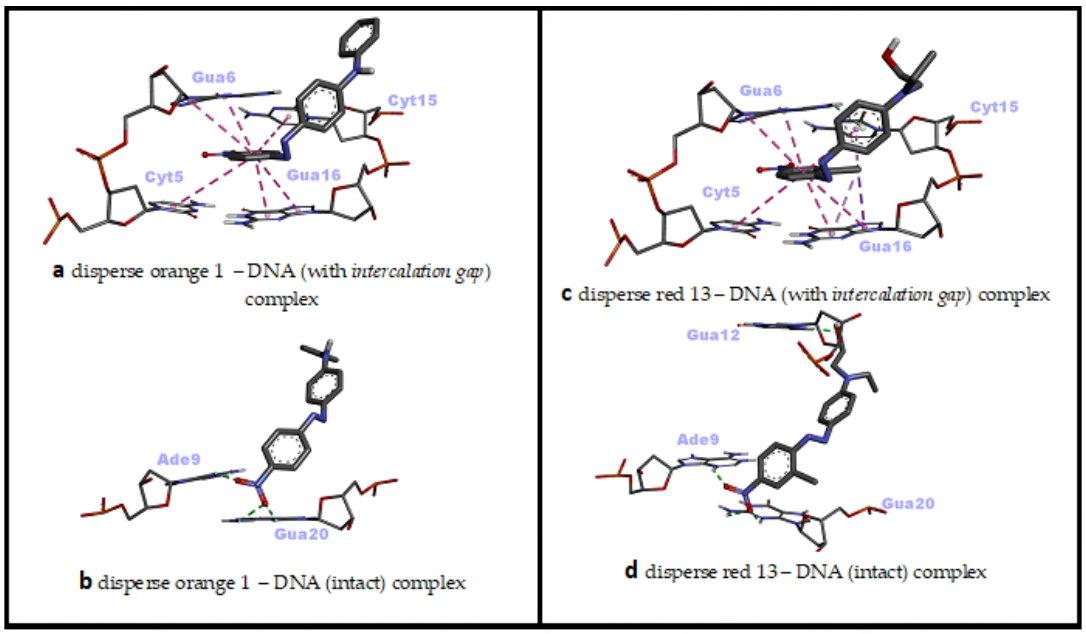

Figure 6. Two-dimensional interaction diagrams of genotoxic azo dyes with dsDNA in two distinct conformations (with and without an *intercalation gap*). dsDNA structures and ligands are depicted in stick mode.

3.3. dsDNA Sequence Selectivity of Top-Ranked Azo Dye Conformations

In this docking study, the determined sequence selectivities (versus two different dsDNA conformations) of the 14 azo dyes in their dominant dsDNA recognition modes are given in Table 3. It has been determined that molecules exhibiting intercalation or threading intercalation mode among 14 azo dyes (p-aminoazobenzene, o-aminoazotoluene, Basic Red 51, CIDB291) preferentially show –CG– or –CGA– sequence selectivity on 20-nucleotide double-stranded dsDNA (PDB ID: 1MKL) having an *intercalation gap* (Table 3). On the other hand, the remaining 10 ligands with the minor groove binding mode being more favorable, (p-dimethylaminoazobenzene, phenazopyridine, Acid Chrome Blue K, Basic Brown 17, Amaranth, Allura Red, Amido Black 10B, CI Disperse Red 1, Disperse Orange 1, Disperse Red 13) specifically and consistently recognized the –TCTGTGGTTG– sequence on the 52-nucleotide double-stranded DNA molecule (PDB ID: 1HJB) and showed –GT– sequence selectivity (p-dimethylaminoazobenzene, phenazopyridine, Acid Chrome Blue K, Basic Brown 17, Amaranth, Amido Black 10B) (Table 3). DNA regions rich in –GT– dinucleotides have been reported as recombinational hotspots [55]. Furthermore, guanine 2-amino group in DNA could be an important contributor in sequence (G-T)-selective DNA binding [56].

In addition, it has been suggested that –GT– sequences (which are more frequent in the euchromatin), found in all eukaryotes, may play a role in the packaging and condensation of DNA into chromosomes, which are supramolecular structures [57,58]. Therefore, DNA regions rich in –GT– dinucleotides may be multifunctional sequences in that they are located in intra- or inter-genic regions where recombination is triggered and they mediate conformational changes of DNA. Binding of the azo dyes at these genomic regions explains why they are able to induce frequent DNA strand breaks, because these dyes, which could bind to DNA in G_1 or S phase, induce single- or double-stranded DNA breaks as a result of the collapse of replication fork [59].

Table 3. dsDNA sequence selectivities of the most favorable binding modes of 14 azo dyes against two different dsDNA conformations.

Dye (Ligand)	Most Favorable Binding Mode	BFE (kcal/mol)	dsDNA Sequence Selectivity
P-aminoazobenzene	Intercalation	−6.49	ACAT**CG**ATCT TGTA**GC**TAGA
O-aminoazotoluene	Threading intercalation	−6.92	ACAT**CGA**TCT TGTA**GC**TAGA
P-dimethylaminoazobenzene	Minor groove	−6.66	GAAGATTTCCAAACTCT**GT**GGTTGCG CTTCTAAAGGTTTGAG**A**CACCAACGC
Phenazopyridine	Minor groove	−6.94	GAAGATTTCCAAACTCT**GTG**GTTGCG CTTCTAAAGGTTTGAG**A**CACCAACGC
Acid Chrome Blue K	Minor groove	−9.36	GAAGATTTCCAAACTCT**GTG**GTTGCG CTTCTAAAGGTTTG**AG**A**CA**CCAACGC
Basic Red 51	Threading intercalation	−6.94	ACAT**CGA**TCT TGTA**GC**TAGA
Basic Brown 17	Minor groove	−8.79	GAAGATTTCCAAACT**CTGT**GGTTGCG CTTCTAAAGGTTTG**A**G**A**CACCAACGC
Amaranth	Minor groove	−9.42	GAAGATTTCCAAACTC**T**GT**GG**TTGCG CTTCTAAAGGTTTGA**GA**C**A**CCAACGC
Allura Red	Minor groove	−8.80	GAAGATTTCCAAACTCT**G**T**GG**TTGCG CTTCTAAAGGTTTGA**GA**C**A**CCAACGC
C.I. Disperse Blue 291	Threading intercalation	−7.39	ACAT**CG**ATCT TGT**AGC**TAGA
Amido Black 10B	Minor groove	−9.23	GAAGATTTCCAAACTCTGTG**GTTG**CG CTTCTAAAGGTTTGAGACAC**C**A**A**CGC
C.I. Disperse Red 1	Minor groove	−7.67	GAAGATTTCCAAACTCTGT**GG**TTGCG CTTCTAAAGGTTTGA**GA**C**A**CCAACGC
Disperse Orange 1	Minor groove	−8.23	GAAGATTTCCAAACTCTGT**G**GTTGCG CTTCTAAAGGTTTGAGAC**A**CCAACGC
Disperse Red 13	Minor groove	−7.68	GAAGATTTCCAAACTCTGT**G**GTTGCG CTTCTAAAGGTTTGA**G**AC**A**CCAACGC

BFE—binding free energy (kcal/mol).

In line with our observations on the minor groove recognition by certain azo dyes, it has been reported that the azo dye "carmoisine" showed specific affinity for the DNA minor groove and bound to the AT-rich region in an experimental study using various biophysical techniques [60]. The sequence of DNA used in that study is not identical to the sequence of intact DNA (1hjb) that we selected in our docking study. Thus, the sequence specificity resulting from binding to the minor groove of DNA may differ in DNAs with different nucleotide sequences.

Finally, we think it would be useful to mention the following regarding the docking calculations we employed in our study: in this study, a "rigid receptor–flexible ligand" docking protocol was applied; therefore, a certain degree of flexibility was allowed on the rotatable bonds of azo dyes during docking, while no conformational plasticity could be simulated in two different dsDNA receptors. Therefore, conformational changes in dsDNA before or upon ligand binding could not be taken into account in this study. For this reason, the docking protocol we used can be considered as a representation of the initial static

interactions between the azo dyes and dsDNA receptors. In other words, target flexibility should also be provided (e.g., molecular dynamics) in order to more clearly explain the role of structural features of DNA, such as twist, rise or groove width, in ligand binding, and to determine the time-dependent evolution and stability of resulting DNA–ligand interactions [24,61].

4. Conclusions

Azo dyes have very attractive vivid colors and are the most widely used and structurally diverse group of commercial organic dyes [62]. Approximately more than 2000 azo dyes are used today which are colorants of materials such as synthetic and natural textile fibers, plastic, leather, hair dyes, waxes and certain petroleum products [63]. In this computational docking study investigating the dsDNA binding interactions and affinity of 14 genotoxic azo dyes—which have been previously known to negatively interact with dsDNA—we showed that most of these dyes are preferentially minor groove binders; however, intercalative binding is also an effective dsDNA recognition mode of a small number of these azo dyes. We determined that the molecular moiety of these dyes that play a primary role in the most favorable binding conformations with dsDNA are the azo, nitro, hydroxyl, ammonium, sulfonate, naphthalene, methoxyphenyl, bromine, nitrophenyl, imidazole, amino-phenylethanol and chloro-nitrophenyl groups. These dyes, which exhibit binding energies ranging from −6.35 kcal/mol to −9.42 kcal/mol against the dsDNA molecule, show specific affinity for GT-rich regions (Tables 2 and 3). The ring structures in the molecular scaffolds of these 14 dyes, which have the ability to form tight binding complexes with dsDNA, as well as some polar groups (such as the hydroxyls and sulfonates) are the critical features for genotoxic dsDNA binding. We are of the opinion that these genotoxic azo dyes, which are frequently used in industrial, health and cosmetic fields, may be banned or non-genotoxic congeners should be immediately produced by further molecular optimization.

Funding: This research received no external funding.

Supplementary Materials: The following supporting information can be downloaded at: https://www.mdpi.com/article/10.3390/colorants1020015/s1, Table S1: Docking results for azo dyes with AutoDock Vina, showing the binding affinity scores for all poses of ligands and the difference in structure (RMSD) against dsDNA with an intercalation gap and intact dsDNA.

Institutional Review Board Statement: Not applicable.

Informed Consent Statement: Not applicable.

Data Availability Statement: The data presented in this study are available on reasonable request from the corresponding author.

Acknowledgments: We thank Cengiz SARIKURKCU for kindly drawing the two-dimensional structures of genotoxic azo dyes with ChemOffice version 19.1.

Conflicts of Interest: The authors declare no conflict of interest.

References

1. Song, J.M.; Lee, K.H.; Seong, B.L. Antiviral effect of catechins in green tea on influenza virus. *Antivir. Res.* **2005**, *68*, 66–74. [CrossRef] [PubMed]
2. Brown, M.A.; De Vito, S.C. Predicting azo dye toxicity. *Crit. Rev. Environ. Sci. Technol.* **1993**, *23*, 249–324. [CrossRef]
3. Morris, P.J.; Travis, A.S. A history of the international dyestuff industry. *Am. Dyest. Report.* **1992**, *81*, 59.
4. Singh, A.L.; Chaudhary, S.; Kumar, S.; Kumar, A.; Singh, A.; Yadav, A. Biodegradation of Reactive Yellow-145 azo dye using bacterial consortium: A deterministic analysis based on degradable Metabolite, phytotoxicity and genotoxicity study. *Chemosphere* **2022**, *300*, 134504. [CrossRef]
5. Khan, S.; Zeyad, M.T.; Malik, A. Genotoxicity assessment of textile waste contaminated soil and characterization of textile dye degradation by a novel indigenous bacterium Ochrobactrum intermedium BS39. *Chemosphere* **2022**, *299*, 134082. [CrossRef]

6. Rajashekarappa, K.K.; Mahadevan, G.D.; Neelagund, S.E.; Sathynarayana, M.; Vijaya, D.; Mulla, S.I. Decolorization of amaranth RI and fast red E azo dyes by thermophilic Geobacillus thermoleovorans KNG 112. *J. Chem. Technol. Biotechnol.* **2022**, *97*, 482–489. [CrossRef]
7. Halilčević, D.; Dautović, E.; Lelić, M.; Husejnović, M.Š.; Smajlović, A.; Srabović, N.; Softić, A. Cytotoxicity and Genotoxicity of Sunset Yellow and Potassium Sorbate in Jurkat Cell Line. *Int. J. Biochem. Res. Rev.* **2022**, *31*, 1–9. [CrossRef]
8. Sharma, K.; Sharma, P.; Dhiman, S.K.; Chadha, P.; Saini, H.S. Biochemical, genotoxic, histological and ultrastructural effects on liver and gills of fresh water fish Channa punctatus exposed to textile industry intermediate 2 ABS. *Chemosphere* **2022**, *287*, 132103. [CrossRef]
9. Li, Y.; Yang, Y.; Yin, S.; Zhou, C.; Ren, D.; Sun, C. Inedible azo dyes and their analytical methods in foodstuffs and beverages. *J. AOAC Int.* **2018**, *101*, 1314–1327. [CrossRef]
10. Miller, J.A.; Miller, E.C. The carcinogenicity of certain derivatives of p-dimethylaminozobenz in the rat. *J. Exp. Med.* **1948**, *87*, 139–156. [CrossRef]
11. Chung, K.-T.; Cerniglia, C.E. Mutagenicity of azo dyes: Structure-activity relationships. *Mutat. Res. Rev. Genet. Toxicol.* **1992**, *277*, 201–220. [CrossRef]
12. da Cruz Brambilla, C.M.C.; Garcia, A.L.H.; da Silva, F.R.; Taffarel, S.R.; Grivicich, I.; Picada, J.N.; Scotti, A.; Dalberto, D.; Mišík, M.; Knasmüller, S. Amido Black 10B a widely used azo dye causes DNA damage in pro-and eukaryotic indicator cells. *Chemosphere* **2019**, *217*, 430–436. [CrossRef] [PubMed]
13. Fernandes, F.H.; Botasso-Nasciutti, M.O.; Svio, A.L.V.; Souza, L.d.C.M.; Fernandes-Cal, J.R.; Cardoso, F.F.; Fontes, M.R.d.M.; Albuquerque, A.F.; Munari, C.C.; Kummrow, F. In Vivo genotoxicity of a commercial CI Disperse Red 1 dye. *Environ. Mol. Mutagenesis* **2018**, *59*, 822–828. [CrossRef]
14. Oliveira, G.; Ferraz, E.; Chequer, F.; Grando, M.; Angeli, J.; Tsuboy, M.; Marcarini, J.; Mantovani, M.; Osugi, M.E.; Lizier, T.M. Chlorination treatment of aqueous samples reduces, but does not eliminate, the mutagenic effect of the azo dyes Disperse Red 1, Disperse Red 13 and Disperse Orange 1. *Mutat. Res. Genet. Toxicol. Environ. Mutagenesis* **2010**, *703*, 200–208. [CrossRef] [PubMed]
15. Jabeen, H.S.; Mahmood, S.; Anwer, S. Genotoxicity assessment of amaranth and allura red using Saccharomyces cerevisiae. *Bull. Environ. Contam. Toxicol.* **2013**, *90*, 22–26. [CrossRef] [PubMed]
16. Tafurt-Cardona, Y.; Suares-Rocha, P.; Fernandes, T.C.C.; Marin-Morales, M.A. Cytotoxic and genotoxic effects of two hair dyes used in the formulation of black color. *Food Chem. Toxicol.* **2015**, *86*, 9–15. [CrossRef]
17. Wang, Q.-X.; Zhang, X.; Ni, J.-C.; Shi, J.-L.; Gao, F.; Chen, G.-L.; Gao, F. Binding mode and photo-cleavage of an azo dye, acid chrome blue K, to double-stranded DNA. *J. Solut. Chem.* **2012**, *41*, 1185–1196. [CrossRef]
18. Wiesmüller, L.; Ford, J.M.; Schiestl, R.H. DNA damage, repair, and diseases. *J. Biomed. Biotechnol.* **2002**, *2*, 45. [CrossRef]
19. Maluf, S.W.; Martínez-López, W.; da Silva, J. *DNA Damage: Health and Longevity*; Hindawi: London, UK, 2018; Volume 2018.
20. Jackson, S.P.; Bartek, J. The DNA-damage response in human biology and disease. *Nature* **2009**, *461*, 1071–1078. [CrossRef]
21. Alberts, B.; Johnson, A.; Lewis, J.; Raff, M.; Roberts, K.; Walter, P. The structure and function of DNA. In *Molecular Biology of the Cell*, 4th ed.; Garland Science: New York, NY, USA, 2002.
22. Watson, J.D.; Crick, F.H. *The Structure of DNA, Cold Spring Harbor Symposia on Quantitative Biology*; Cold Spring Harbor Laboratory Press: Cold Spring Harbor, NY, USA, 1953; pp. 123–131.
23. Zimmerman, S.B. The three-dimensional structure of DNA. *Annu. Rev. Biochem.* **1982**, *51*, 395–427. [CrossRef]
24. Ricci, C.G.; Netz, P.A. Docking studies on DNA-ligand interactions: Building and application of a protocol to identify the binding mode. *J. Chem. Inf. Modeling* **2009**, *49*, 1925–1935. [CrossRef] [PubMed]
25. Hannon, M.J. Supramolecular DNA recognition. *Chem. Soc. Rev.* **2007**, *36*, 280–295. [CrossRef] [PubMed]
26. Winston, C.T.; Boger, D.L. Sequence-selective DNA recognition: Natural products and nature's lessons. *Chem. Biol.* **2004**, *11*, 1607–1617.
27. Waring, M.J.; Bailly, C. DNA recognition by intercalators and hybrid molecules. *J. Mol. Recognit.* **1994**, *7*, 109–122. [CrossRef]
28. Guo, Y.; Yue, Q.; Gao, B. Molecular docking study investigating the possible mode of binding of CI Acid Red 73 with DNA. *Int. J. Biol. Macromol.* **2011**, *49*, 55–61. [CrossRef]
29. Liman, R.; Ali, M.M.; Ciğerci, İ.H.; İstifli, E.S.; Sarıkurkcu, C. Cytotoxic and genotoxic evaluation of copper oxychloride through Allium test and molecular docking studies. *Environ. Sci. Pollut. Res.* **2021**, *28*, 44998–45008. [CrossRef]
30. Kurt, D.; Acar, A.; Çavuşoğlu, D.; Yalçin, E.; Çavuşoğlu, K. Genotoxic effects and molecular docking of 1, 4-dioxane: Combined protective effects of trans-resveratrol. *Environ. Sci. Pollut. Res.* **2021**, *28*, 54922–54935. [CrossRef]
31. Snyder, R.D.; Holt, P.A.; Maguire, J.M.; Trent, J.O. Prediction of noncovalent Drug/DNA interaction using computational docking models: Studies with over 1350 launched drugs. *Environ. Mol. Mutagen.* **2013**, *54*, 668–681. [CrossRef]
32. Wiedemann, P.M.; Schütz, H. *The Role of Evidence in Risk Characterization: Making Sense of Conflicting Data*; John Wiley & Sons: Hoboken, NJ, USA, 2008.
33. Topaktas, M.; Kafkas, N.; Sadighazadi, S.; Istifli, E. In vitro cytogenetic toxicity of bezafibrate in human peripheral blood lymphocytes. *Cytotechnology* **2017**, *69*, 579–589. [CrossRef]
34. Istifli, E.S.; Çelik, R.; Hüsunet, M.T.; Çetinel, N.; Demirhan, O.; Ila, H.B. cytogenotoxic evaluation of sertraline. *Interdiscip. Toxicol.* **2018**, *11*, 181–188. [CrossRef]
35. Bender, B.J.; Gahbauer, S.; Luttens, A.; Lyu, J.; Webb, C.M.; Stein, R.M.; Fink, E.A.; Balius, T.E.; Carlsson, J.; Irwin, J.J. A practical guide to large-scale docking. *Nat. Protoc.* **2021**, *16*, 4799–4832. [CrossRef] [PubMed]

36. Ma, L.; Wang, J.; Zhang, Y. Probing the characterization of the interaction of aflatoxins B1 and G1 with calf thymus DNA in vitro. *Toxins* **2017**, *9*, 209. [CrossRef] [PubMed]
37. Giri, A. The genetic toxicology of paracetamol and aspirin: A review. *Mutat. Res. Rev. Genet. Toxicol.* **1993**, *296*, 199–210. [CrossRef]
38. Watanabe, M. The cytogenetic effects of aspirin and acetaminophen on in vitro human lymphocytes. *Nippon. Eiseigaku Zasshi* **1982**, *37*, 673–685. [CrossRef] [PubMed]
39. Husain, M.A.; Rehman, S.U.; Ishqi, H.M.; Sarwar, T.; Tabish, M. Spectroscopic and molecular docking evidence of aspirin and diflunisal binding to DNA: A comparative study. *RSC Adv.* **2015**, *5*, 64335–64345. [CrossRef]
40. Loechler, E.L.; Teeter, M.M.; Whitlow, M.D. Mapping the binding site of aflatoxin B1 in DNA: Molecular modeling of the binding sites for the N (7)-guanine adduct of aflatoxin B1 in different DNA sequences. *J. Biomol. Struct. Dyn.* **1988**, *5*, 1237–1257. [CrossRef]
41. Hanwell, M.D.; Curtis, D.E.; Lonie, D.C.; Vandermeersch, T.; Zurek, E.; Hutchison, G.R. Avogadro: An advanced semantic chemical editor, visualization, and analysis platform. *J. Cheminform.* **2012**, *4*, 17. [CrossRef]
42. Lewis-Atwell, T.; Townsend, P.A.; Grayson, M.N. Comparisons of different force fields in conformational analysis and searching of organic molecules: A review. *Tetrahedron* **2021**, *79*, 131865. [CrossRef]
43. Vela, S.; Fabrizio, A.; Briling, K.R.; Corminboeuf, C. Learning the Exciton Properties of Azo-dyes. *J. Phys. Chem. Lett.* **2021**, *12*, 5957–5962. [CrossRef]
44. Brüschweiler, B.J.; Merlot, C. Azo dyes in clothing textiles can be cleaved into a series of mutagenic aromatic amines which are not regulated yet. *Regul. Toxicol. Pharmacol.* **2017**, *88*, 214–226. [CrossRef]
45. Eberhardt, J.; Santos-Martins, D.; Tillack, A.; Forli, S. AutoDock Vina 1.2. 0: New docking methods, expanded force field, and Python bindings. *J. Chem. Inf. Model.* **2021**, *61*, 3891–3898. [CrossRef] [PubMed]
46. Morris, G.M.; Huey, R.; Lindstrom, W.; Sanner, M.F.; Belew, R.K.; Goodsell, D.S.; Olson, A.J. AutoDock4 and AutoDockTools4: Automated docking with selective receptor flexibility. *J. Comput. Chem.* **2009**, *30*, 2785–2791. [CrossRef] [PubMed]
47. Tsuda, S.; Matsusaka, N.; Madarame, H.; Ueno, S.; Susa, N.; Ishida, K.; Kawamura, N.; Sekihashi, K.; Sasaki, Y.F. The comet assay in eight mouse organs: Results with 24 azo compounds. *Mutat. Res. Genet. Toxicol. Environ. Mutagenesis* **2000**, *465*, 11–26. [CrossRef]
48. Levine, W.G. Metabolism of azo dyes: Implication for detoxication and activation. *Drug Metab. Rev.* **1991**, *23*, 253–309. [CrossRef]
49. Stiborová, M.; Frei, E.; Schmeiser, H.H.; Wiessler, M.; Hradec, J. Formation and 32P-postlabeling of DNA and tRNA adducts derived from peroxidative activation of carcinogenic azo dye N, N-dimethyl-4-aminoazobenzene. *Carcinogenesis* **1992**, *13*, 1657–1662. [CrossRef]
50. Stiborová, M.; Asfaw, B.; Frei, E. Peroxidase-activated carcinogenic azo dye Sudan I (Solvent Yellow 14) binds to guanosine in transfer ribonucleic acid. *Gen. Physiol. Biophys.* **1995**, *14*, 39.
51. Mpountoukas, P.; Pantazaki, A.; Kostareli, E.; Christodoulou, P.; Kareli, D.; Poliliou, S.; Mourelatos, C.; Lambropoulou, V.; Lialiaris, T. Cytogenetic evaluation and DNA interaction studies of the food colorants amaranth, erythrosine and tartrazine. *Food Chem. Toxicol.* **2010**, *48*, 2934–2944. [CrossRef]
52. de Aragão Umbuzeiro, G.; Freeman, H.; Warren, S.H.; Kummrow, F.; Claxton, L.D. Mutagenicity evaluation of the commercial product CI Disperse Blue 291 using different protocols of the Salmonella assay. *Food Chem. Toxicol.* **2005**, *43*, 49–56. [CrossRef]
53. Uliana, C.V.; Garbellini, G.S.; Yamanaka, H. Evaluation of the interactions of DNA with the textile dyes Disperse Orange 1 and Disperse Red 1 and their electrolysis products using an electrochemical biosensor. *Sens. Actuators B Chem.* **2013**, *178*, 627–635. [CrossRef]
54. Weisburger, J.H. A perspective on the history and significance of carcinogenic and mutagenic N-substituted aryl compounds in human health. *Mutat. Res.* **1997**, *376*, 261–266. [CrossRef]
55. Stallings, R.; Ford, A.; Nelson, D.; Torney, D.; Hildebrand, C.; Moyzis, R. Evolution and distribution of (GT) n repetitive sequences in mammalian genomes. *Genomics* **1991**, *10*, 807–815. [CrossRef]
56. Kuwahara, J.; Sugiura, Y. Sequence-specific recognition and cleavage of DNA by metallobleomycin: Minor groove binding and possible interaction mode. *Proc. Natl. Acad. Sci.* **1988**, *85*, 2459–2463. [CrossRef] [PubMed]
57. Gross, D.S.; Garrard, W.T. The ubiquitous potential Z-forming sequence of eucaryotes,(dT-dG) n.(dC-dA) n, is not detectable in the genomes of eubacteria, archaebacteria, or mitochondria. *Mol. Cell. Biol.* **1986**, *6*, 3010–3013. [PubMed]
58. Umezawa, Y.; Nishio, M. Thymine-methyl/π interaction implicated in the sequence-dependent deformability of DNA. *Nucleic Acids Res.* **2002**, *30*, 2183–2192. [CrossRef] [PubMed]
59. Ooka, M.; Kobayashi, K.; Abe, T.; Akiyama, K.; Hada, M.; Takeda, S.; Hirota, K. Determination of genotoxic potential by comparison of structurally related azo dyes using DNA repair-deficient DT40 mutant panels. *Chemosphere* **2016**, *164*, 106–112. [CrossRef]
60. Basu, A.; Suresh Kumar, G. Minor groove binding of the food colorant carmoisine to DNA: Spectroscopic and calorimetric characterization studies. *J. Agric. Food Chem.* **2014**, *62*, 317–326. [CrossRef]
61. Ferreira, L.G.; Dos Santos, R.N.; Oliva, G.; Andricopulo, A.D. Molecular docking and structure-based drug design strategies. *Molecules* **2015**, *20*, 13384–13421. [CrossRef]
62. Chung, K.-T. Azo dyes and human health: A review. *J. Environ. Sci. Health Part C* **2016**, *34*, 233–261. [CrossRef]
63. Moosvi, S.; Kher, X.; Madamwar, D. Isolation, characterization and decolorization of textile dyes by a mixed bacterial consortium JW-2. *Dye. Pigment.* **2007**, *74*, 723–729. [CrossRef]